

Bidisperse Aggregation and Gel Formation via Simultaneous Convection and Diffusion

Ian J. Laurenzi[†] and Scott L. Diamond^{*}

Department of Chemical Engineering, Institute for Medicine and Engineering, University of Pennsylvania, Philadelphia, Pennsylvania 19104

Stochastic simulations are performed for two-component transport-limited aggregation processes with Brownian motion and shear contributing to the collision frequency. To study the effects of both mechanisms, the radius ratio of the initially pure particles is 1:8 on average, with the larger particles having sizes on the order of microns (μm). For a mixed orthokinetic–perikinetic kernel, the kinetics of the aggregation process and gel point are shown to have a cooperative dependence on shear and the relative concentration of large particles to small ones. This was found to be a result of the shear sensitivity of the aggregation process to the addition of large particles. Ultimately, it is shown that accurate prediction of the kinetics and gel points of complex aggregation phenomena requires the use of the stochastic approach to the aggregation kinetics upon which the simulations are based.

Introduction

The aggregation of particles into larger structures is a ubiquitous phenomenon of interest to a broad range of researchers, characterizing processes from blood coagulation to nanoparticle formation. In liquids, transport-limited clustering of solute particles can be brought about by shearing the solution, by gravitational settling, or, depending on the size of the particles, by Brownian motion. Whereas most studies of the kinetics of aggregation focus on just one transport mechanism, many real aggregation processes feature several modes of transport, such as shear and diffusion. However, the consequences of multiple transport mechanisms on the kinetics of aggregation processes have never been fully quantified.

Further complicating the analysis of transport-limited aggregation is the fact that multiple components are often involved. For instance, the process of heterogeneous aggregation often occurs in conjunction with homogeneous nucleation processes, augmenting the rate at which clouds and aerosols form.¹ However, the subject of multicomponent aggregation has been sparsely addressed in the literature, with a few papers on this subject addressing a physical system.^{2,3}

The state of an aggregation process can be expressed in terms of its particle size distribution (PSD), which characterizes the average particle size, polydispersity, and onset of gelation. The quantitative approach to its dynamics was developed by Smoluchowski, whose kinetic theory of clustering remains the basis of almost all theoretical treatment of aggregation kinetics.⁴ The kinetic theory directly gives Smoluchowski's population balance equation (PBE) for single-component aggregation

$$\frac{\partial c(i,t)}{\partial t} = \frac{1}{2} \sum_{j=1}^{i-1} K(j,i-j) c(j,t) c(i-j,t) - \sum_{j=1}^{\infty} K(i,j) c(i,t) c(j,t) \quad (1)$$

In eq 1, the first term on the RHS is the sum of all of the rates of aggregations yielding particles composed of i monomers. The second term is the sum of the rates of aggregation of i -mers to form larger particles. The quantity $K(i,j)$ is denoted the kernel of the process and acts as a “second-order rate constant” for the “reaction” $(i) + (j) \rightarrow (i+j)$. Each aggregation mechanism features a unique kernel that can be derived from consideration of the transport and chemistry of suspended particles. Hence, the kernel embeds the microphysical mechanism of the process into Smoluchowski's equation.

This approach can be expanded to address the conservation of multiple components. In such cases, two or more population balances must be incorporated into a mass-action equation such as eq 1. For example, Lushnikov's equation for the aggregation of particles composed of two components is⁵

$$\frac{\partial \tilde{c}(u,v;t)}{\partial t} = \frac{1}{2} \int_0^u \int_0^v K(u-u',v-v' | u',v') \tilde{c}(u-u',v-v';t) \tilde{c}(u',v';t) dv' du' - \int_0^{\infty} \int_0^{\infty} K(u,v | u',v') \tilde{c}(u,v;t) \tilde{c}(u',v';t) dv' du' \quad (2)$$

Here, $K(u,v | u',v')$ is a multicomponent kernel and $\tilde{c}(u,v;t)$ is a concentration density for the system. The concentration of particles with compositions $(<u, <v)$ can be determined from $\tilde{c}(u,v;t)$ by integration

$$G(u,v;t) = \int_0^u \int_0^v \tilde{c}(u,v;t) du dv \quad (3)$$

Because of the mathematical forms of most kernels, only a few analytical solutions are known to exist.^{4,6,7,8} Furthermore, the differential and integral complexity of eqs 1 and 2 makes numerical approximation difficult

^{*} Author to whom correspondence should be addressed. E-mail: sld@seas.upenn.edu. Phone: (215) 573-5702. Fax: (215) 573-7227.

[†] E-mail: laurenzi@seas.upenn.edu.

and often coarse. Fortunately, these difficulties can be alleviated by a paradigm shift. In a recent publication, a new approach was developed for aggregation kinetics of multicomponent particles based on the theory of Markov processes.^{2,9} Akin to the stochastic approach to chemical kinetics,¹⁰ this methodology features *probabilistic* evolution of the state of a system according to the same laws dictating the evolution of the real process. Consequently, the stochastic approach naturally lends itself to *exact* Monte Carlo (MC) simulation. Because the kernel is at the heart of the stochastic approach as well, it parallels Smoluchowski's deterministic approach, predicting, on average, the same behaviors for *any* aggregation processes. Furthermore, it yields a more exact treatment of gel phenomena, accounting explicitly for the mass of an aggregating system.

Although the effects of shear and diffusion on aggregation kinetics have been studied experimentally for single-component systems, a complete mathematical analysis of the size distribution and its moments has never been conducted. In this paper, the versatility of the stochastic approach is employed to quantify the kinetics of two-component aggregation between micron- and submicron-sized particles differentially subjected to both shear and Brownian transport mechanisms. In so doing, the effects of changing the relative concentrations of the two components are investigated to develop a quantitative approach to the characterization of aggregation kinetics and gel formation.

Methods

Stochastic Simulation Algorithm. As with the deterministic approach, the stochastic approach is concerned with the evolution of the states of an aggregating system, defined by the types of particle species and their populations or concentrations. However, it is the *probability* of a state that is specified by the stochastic master equations. A stochastic master equation for an aggregating system can be written as

$$\frac{d\mathcal{P}}{dt} = \mathcal{A}\mathcal{P} \quad (4)$$

In eq 4, \mathcal{P} is a vector of probabilities $\{\mathcal{P}_n\}$ that the system will be in the n th state at time t , where states are defined by specific PSDs. \mathcal{A} is the transition matrix for the stochastic process, where $\{\mathcal{A}_{mn} dt\}$ represents the probabilities that the system will go from the m th state to the n th state in the next differential time period dt . By solution of master equations such as eq 4 and appropriate averaging of the time-dependent probabilities $\mathcal{P}(t)$, the stochastic time evolution of the PSD can be predicted. However, the real power of the stochastic approach is not in its capacity to predict the probabilities of states, but in its probabilistic description of the process. That is, given the transition probabilities $\{\mathcal{A}_{mn} dt\}$, MC simulation of the aggregation process can be performed. The method used to implement the numerical algorithm follows.

Consider a batch aggregation process in a volume V in which there are initially N "particle species". Let a species be defined as a type of particle with a unique composition (u, v, \dots) , where u, v , etc., are conserved size variables for each component, such as the mass or volume. Subsequently, let each state be defined by the populations $X_i \in \mathcal{N}$ of each unique species $i \in [1, M]$. Because the particles of these species are uniformly

randomly distributed throughout V , they will randomly collide with and adhere to each other. Thus, transition probabilities for aggregation events can be written as

$$C(i,j) dt = \text{probability that a specific pair of particles of species } i \text{ and } j \text{ will aggregate in the next } dt \quad (5)$$

The probabilities that any two particles will aggregate will depend on the populations of the aggregating species. For example, there are $X_i X_j$ ways that two different species i and j can aggregate and $\binom{X_i}{2}$ ways that species i can aggregate with itself. Hence

$$a(i,j) dt = C(i,j) X_i X_j dt = \text{probability that any two particles of species } i \text{ and } j (i \neq j) \text{ will aggregate in the next } dt \quad (6)$$

$$a(i,i) dt = C(i,i) \binom{X_i}{2} dt = \text{probability that any two particles of species } i \text{ will homo-aggregate in the next } dt \quad (7)$$

Furthermore, it can be shown that^{2,11}

$$C(i,j) \equiv \frac{K(i,j)}{V} \quad (8)$$

where, in contrast to the definition given in eq 1, $K(i,j)$ is the kernel between *species* i and j . That is, if species i is defined by the composition (u, v) , and species j by (u', v') , then $K(i,j) = K(u, v | u', v')$, as in eq 2. Because states can change only by individual aggregation events, it follows that eqs 6 and 7 are examples of the aforementioned transition probabilities from which the stochastic simulation algorithm is derived.

The method of simulation of the kinetics of the aggregation process requires two steps: probabilistic selection of the time until the next aggregation event and probabilistic selection of which event it will be. Using eqs 6 and 7, probability distributions can be derived for both the quiescence time and the imminent event, from which values can be drawn by MC. Laurenzi and Diamond^{2,9} and Gillespie^{12,13} give a detailed derivation of these distributions and an efficient algorithm drawn from them.

The algorithm consists of the following steps: First, a set of species must be defined according to an initial particle density $\tilde{\chi}(u, v; 0)$. To do this, a batch volume V must be specified such that the initial number of particles is $X_0 = V \times G(\infty, \infty; 0)$. Subsequently, by standard MC sampling of the normalized distribution $\tilde{\chi}(u, v; 0)/G(\infty, \infty; 0)$, an initial set of particles can be chosen in accordance with the initial distribution $\tilde{\chi}(u, v; 0)$ (Appendix). In principle, the initial species could be represented by these particles, producing X_0 singly populated species. A more efficient approach discretizes the size spaces u and v into \mathcal{M} and \mathcal{N} bins defined by linearly distributed abscissas u_j ($j \in [1, \mathcal{M}]$) and v_k ($k \in [1, \mathcal{N}]$) and sorts the MC-defined particles into these bins. As a result, the number of species is reduced from X_0 to $N = \mathcal{M} \times \mathcal{N}$. The initial species $i \in [1, N]$ are subsequently defined as having

$$\bar{u}_i = \frac{1}{2}(u_{j-1} + u_j) \quad (9)$$

and

$$\bar{v}_i = 1/2(v_{k-1} + v_k) \quad (10)$$

of the first and second components, and populations defined by the number of particles falling in the j th u bin and k th v bin.

With the initial state defined, the quiescence time until the first event can be selected via the following equation

$$\tau = \frac{1}{\alpha} \ln\left(\frac{1}{r_1}\right) \quad (11)$$

where r_1 is a uniform random number on (0, 1] and α is defined by

$$\alpha = \sum_{i=1}^N \sum_{j=1}^I a(i,j) \quad (12)$$

Next, the species involved in the imminent event are chosen by the following inequality

$$\sum_{i=1}^{\mu-1} \sum_{j=1}^{v-1} a(i,j) \leq r_2 \alpha \leq \sum_{i=1}^{\mu} \sum_{j=1}^v a(i,j) \quad (13)$$

where r_2 is another uniform random number on (0, 1]. The selection of the aggregating species can be implemented by sequential addition of $a(i,j)$ until $r_2\alpha$ is exceeded. Furthermore, it is independent of the ordering of the summation, inasmuch as the selection is probabilistic. The process of selection of μ and ν can be optimized by the use of special data structures in order to reduce the number of computations in eqs 12 and 13.⁹

After selection of a quiescence time and pair of aggregating species, a time counter is incremented by τ , and populations of the "reactant" species μ and ν and "product" species π are adjusted. Subsequently, all transition probabilities depending on X_μ , X_ν , and X_π are updated to reflect the current state of the system, and the process is repeated. When a species is depopulated, it is removed from the list of species, and its aggregation information (C , a) is purged from memory. Likewise, when a new species is created, N is incremented, the new species is added to the end of the list of species, and its aggregation events $a(N, j)$ ($j \in [1, N]$) are generated.

Computation of Moments. Often, the most important quantities used in the characterization of aggregation kinetics are not the particle distributions $\hat{\chi}(u, v, t)$ themselves but their moments, defined as

$$M_{j,k}(t) = \int_0^\infty \int_0^\infty u^j v^k \hat{\chi}(u, v, t) du dv \quad (14)$$

for systems with two components. In systems with one component, the moments of interest are $M_0(t)$, $M_1(t)$, and $M_2(t)$, which are the total number of particles, total mass of particles, and distribution width, respectively. In a multicomponent system, the quantities $M_{0,0}(t)$, $M_{1,0}(t)$, and $M_{0,1}(t)$ give the total numbers of particles, the total mass of the first component, and the total mass of the second component, respectively. As in the single-component case, higher moments can be used to predict the width and breadth of particle distributions to various degrees, as well as the propensity of a system to exhibit a gel transition. For example, $M_{0,2}$ is the

variance of the distribution in the second component size (v), $M_{1,1}$ the covariance, etc. Prior to complete aggregation, at which point there is only a single particle, the increase of these parameters over time reflects the distribution of the particles across the heterotypic size space.

Definition of the moments of the distributions predicted by MC is similar to eq 14. Because the stochastically generated states defined by the MC simulation are tantamount to integrals of $\hat{\chi}(u, v, t)$, the moment integral can be expressed as

$$\int_0^u \int_0^v u' v' \hat{\chi}(u, v, t) du dv = \sum_{i=1}^N \bar{u}_i^j \bar{v}_i^k X_i \theta(u - \bar{u}_i) \theta(v - \bar{v}_i) \quad (15)$$

where $\theta(x)$ is the unit step function. Hence, by summation of the weighted populations of species i with $\bar{u}_i \leq u$ and $\bar{v}_i \leq v$, all moments of the MC-predicted PSD can be computed exactly.

Kernels. Diffusion is a factor in every transport-limited aggregation process, inasmuch as Brownian motion has the potential to bring particles into intimate contact. In liquids at ambient temperatures, the diffusive mechanism is most important for particles with diameters on the order of nanometers. The perikinetic kernel for a pair of species defined by the compositions (u, v) and (u', v'), where the total volume of the first species is ($u + v$) and the total volume of the second is ($u' + v'$), is

$$K_D(u, v | u', v') = \epsilon(u, v | u', v') \frac{2k_B T}{3\eta} \left[2 + \left(\frac{u+v}{u'+v'}\right)^{1/3} + \left(\frac{u+v}{u'+v'}\right)^{-1/3} \right] \quad (16)$$

In this expression, k_B is Boltzmann's constant, T is the temperature, and μ is the solution viscosity. In eq 16, the aggregates formed are not assumed to be fractal, resulting in the exponents of $1/3$. The quantity $k_B T/\eta$ is a ratio of the thermal energy to the solution viscosity and is equal to 4.037×10^{-12} cm³/s at 20 °C when the particles aggregate in aqueous solution. As its name suggests, the sticking probability $\epsilon_D(u, v | u', v') \in (0, 1]$ gives the probability of adhesion between particles of compositions (u, v) and (u', v'), given that they collide. Because of the dependence of this probability on the chemical kinetics of bond formation between or charge distributions of the aggregating particles, it is potentially a function of both size and composition. In our simulations, it is been set as a constant.

Unlike Brownian objects, particles with radii on the order of microns can have their transport affected by fluid convection. The orthokinetic kernel for the shear-mediated aggregation of particles is

$$K_S(u, v | u', v') = \epsilon(u, v | u', v') \frac{G}{\pi} [(u+v)^{1/3} + (u'+v')^{1/3}]^3 \quad (17)$$

where, again, $\epsilon(u, v | u', v')$ is the sticking probability and G is the shear rate of the solution. Because eq 17 is based on a linear trajectory model of shear-induced collision, it fails to account for hydrodynamic interactions between approaching particles, which can diminish the actual collision rate.^{14,15} Thus, the *effective* sticking probability for shear-mediated collision $\epsilon_S(u, v | u', v')$ includes corrections for hydrodynamic resistance (curvilinear trajectories) and can be less than unity in

practice as a consequence of shear rate dependence of the actual collision rate. Although this would result in differences in the effective sticking probabilities for the perikinetic and orthokinetic kernels, we have assumed that hydrodynamic resistance is negligible in this study and set $\epsilon_S(u, v | u', v') = \epsilon_D(u, v | u', v') = \epsilon$ for general testing of the MC method.

In the region between the Brownian-dominated and shear-dominated regimes, both modes of transport can contribute to the rate of aggregation. Complex rate kernels have been derived for this case^{14,16} predicting higher aggregation rates than the sum predicted by each regime. However, direct experiments conducted by Swift and Friedlander (1964)¹⁷ have demonstrated that the kernel for mixed transport behaves to a high degree of accuracy as a linear combination of eqs 16 and 17

$$K(u, v | u', v') = K_S(u, v | u', v') + K_D(u, v | u', v') \quad (18)$$

For very small particles, the diffusive term dominates, whereas large particles are dominated by the shear term of the kernel. We note that neither Smoluchowski's equation (eq 1) nor Lushnikov's equation (eq 2) have been solved exactly for this combined kernel.

Simulation Results and Discussion

Single-Component Simulations. Simulations of single-component aggregation processes mediated by shear and diffusion were conducted according to the experimental conditions of Swift and Friedlander.¹⁷ In brief, simulations of identical spherical particles of 0.871 μm diameter at a concentration of $c_0 = 2.0 \times 10^8$ particles/cm³ were conducted at $G = 1, 5, 20, 40,$ and 80 s^{-1} , with $kT\eta = 4.526 \times 10^{-12} \text{ cm}^3/\text{s}$ and $\epsilon = 0.364$. Results of these simulations are given in Figure 1, which is identical to Figures 10 and 11 of Swift and Friedlander.¹⁷ In accordance with their experimental results, the numbers of particles in the simulations are approximately given by the expression

$$\ln \left[\frac{M_0(t) + P}{M_0(t)} \right] \left(\frac{M_0(0)}{M_0(0) + P} \right) = \frac{4\epsilon G \phi}{\pi} t \quad (19)$$

where $P = 3G\phi\eta/\pi kT$ and ϕ is the volume fraction of the particles. Despite the slight curvature of the data in Figure 1a, linear regression gives R^2 values in excess of 0.99 at each shear rate. By use of a quadratic fitting function, estimates of the initial slopes of the curves were computed and plotted against their corresponding values of G in Figure 1b. As predicted by eq 19, the slopes were found to be linear and in accordance with the results of Swift and Friedlander.¹⁷

Bidisperse Simulations. Simulations of two-component aggregation processes were conducted with the bivariate size distribution density

$$\delta(u, v; 0) = c_1 \frac{1}{\beta_1 \beta_2} \frac{\left(\frac{u}{\beta_1}\right)^{\alpha_1 - 1} \exp\left(-\frac{u}{\beta_1}\right)}{\Gamma(\alpha_1)} \delta\left(\frac{v}{\beta_2}\right) + c_2 \frac{1}{\beta_1 \beta_2} \frac{\left(\frac{v}{\beta_2}\right)^{\alpha_2 - 1} \exp\left(-\frac{v}{\beta_2}\right)}{\Gamma(\alpha_2)} \delta\left(\frac{u}{\beta_1}\right) \quad (20)$$

This density represents two pure and distinct types of particles, each with a unique size distribution. We have

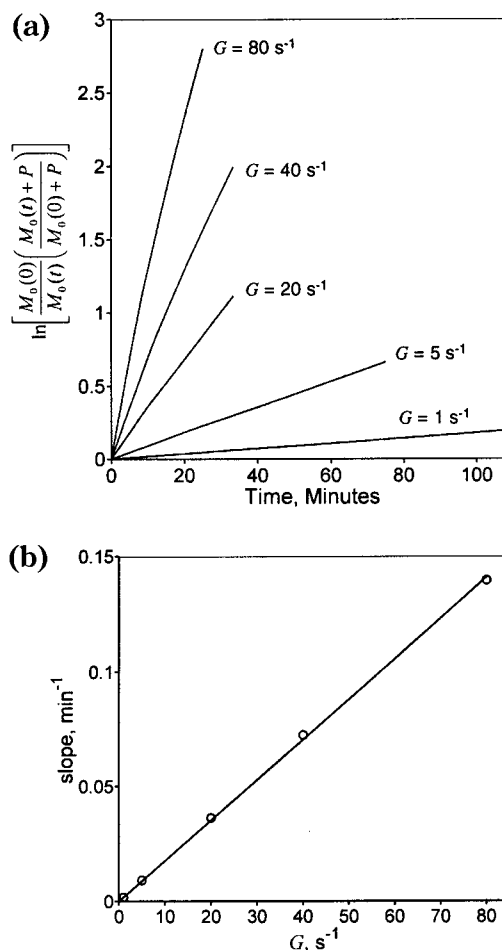


Figure 1. Results of simulations of Swift and Friedlander's¹⁷ experiments on shear coagulation of a monodisperse latex dispersion. (a) Almost-straight lines are obtained, in agreement with the experimental results and eq 19. (b) The initial slopes of the lines in a are proportional to G , as predicted by experiment and eq 19.

chosen these to be broad gamma distributions with $\alpha_1 = 2$, $\alpha_2 = 8$, $\beta_1 = 3.49 \times 10^{-14} \text{ cm}^3$, and $\beta_2 = 4.47 \times 10^{-12} \text{ cm}^3$, such that the average volumes of the two pure particle types were $6.98 \times 10^{-14} \text{ cm}^3$ and $3.58 \times 10^{-11} \text{ cm}^3$. The initial concentrations of the two particle types were varied relative to the constraint $c_1 + c_2 = c_0 = 2.5 \times 10^{10}$ particles/cm³, so as to keep the total concentration of particles constant and dilute over all simulated conditions. As both the PBE and eq 11 show that time scales with $(c_0\epsilon)^{-1}$, the simulation results in Figures 2–5 have been plotted against the dimensionless time scale $t^* = \epsilon c_0(kT/\mu)t$.

The parameters for the initial size distribution are chosen to ensure that the particles can aggregate by both shear and diffusion. Initially, the average Peclet numbers for the two particle types

$$Pe_{ij} = \frac{3\pi\eta(R_i + R_j)^3 G}{kT} \quad (21)$$

are $Pe_{1,1} = 0.31$, $Pe_{1,2} = 28$, and $Pe_{2,2} = 159$ at $G = 1.0 \text{ s}^{-1}$ and $kT\eta = 4.037 \times 10^{-12} \text{ cm}^3/\text{s}$. Thus, simulations are performed at shear rates of 0, 1.0, and 10.0 s^{-1} to span the range of Brownian- and shear-dominated transport. Furthermore, the initial particle fraction of component 2 particles, $\xi = c_2/c_0$, has been varied to adjust the amount of each type of transport at a given

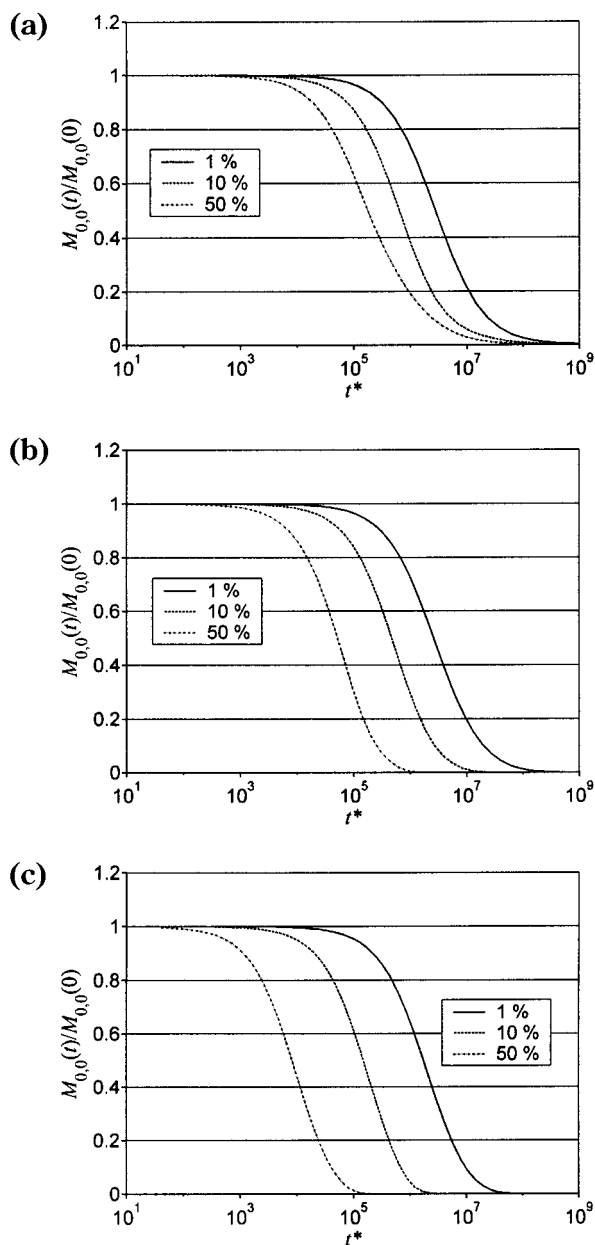


Figure 2. Particle conversion for aggregation of mixtures of Brownian (255 nm) and microscopic (2.04 μm) particles at shear rates $G =$ (a) 0, (b) 1.0, and (c) 10.0 s^{-1} , where 1–50% of the initial particles are of the larger type.

shear rate. Figures 2–5 give the average results of 10 simulations of this aggregation process.

Particle Consumption. The time dependence of the normalized zeroth moment of the size distribution representing the conversion of particles is given in Figure 2. In the absence of shear, there is almost no dependence of the aggregation process on ξ because the diffusion kernel has a weak dependence on the *total* size. As eq 16 shows, perikinetic aggregation is a function of the *relative* size. Because the initial average relative ratio of radii is 1:8, heterotypic aggregation is faster than homotypic processes. The relative difference in rates is even more dramatically pronounced as the concentrations of small and large particles approach each other ($\xi = 50\%$) via the combinatorial weighting in eqs 6 and 7. However, the rapid heterotypic aggregation exhausts itself at about 10 s into the process as the particles homogenize.

As the shear rate is increased from 0 to 10 s^{-1} , the perikinetic kernel is progressively dominated by the orthokinetic kernel. However, because $Pe_{1,1} = 3.1$, Brownian aggregation is still competitive for component 1 particles. Consequently, when $\xi = 1\%$, the consumption of particles over the range of shear studied is approximately constant. However, when ξ is increased to 10 or 50%, particle consumption is dramatically increased, with changes in the half-lives of orders of magnitude. In these cases, the products of large species populations (eqs 6 and 7) augment the speed of the orthokinetic process. As shear rate is increased to 100 s^{-1} and beyond, the consumption curve shifts dramatically to the left, even for $\xi = 1\%$, as orthokinetic aggregation results in huge aggregates of component 2 particles that serve as diffusive sinks for component 1 particles, owing to the size gradient. However, at these high shear rates, experimentation has shown that fragmentation plays an important role in the aggregation process;^{18–20} hence, the simulation for this irreversible aggregation model is not expected to apply to systems in this shear regime.

Gel Formation. In Figures 3–5, the dynamics of the normalized second moments $M_{2,0}$, $M_{0,2}$, and $M_{1,1}$, respectively, are given. These moments collectively denote the width and breadth of the bivariate particle size distribution. Consequently, because of the variation of the relative concentrations of the two components, Figures 3a and 4a show variation in the initial values of the second moments. However, because there are no mixed aggregates initially, $M_{1,1}$ is initially zero for all shear rates and initial concentrations of particles. As time progresses, the second moments increase as functions of both shear and relative concentration, reflecting the increase in polydispersity in each component. The similarities of Figures 3–5 reflect the fact that there is no explicit composition dependence of the aggregating particles in eq 18.

Because aggregation is treated as irreversible in our simulations, the normalization of the second moments $M_{2,0}/M_{1,0}^2$, $M_{0,2}/M_{0,1}^2$, and $M_{1,1}/(M_{0,1}M_{1,0})$ reflects the fact that, upon complete aggregation of all particles, the quotients must physically equal unity. Whereas this behavior is intuitive, it differs from the results of the PBE, which predict divergence of the second-order moments at $t \leq \infty$. This discrepancy results from two approximations implicit in the derivation of the deterministic approach. The first of these is that deterministic prediction of the aggregation process requires that matter be treated as continuous. Furthermore, the stochastic fluctuations of the kinetics of singly populated species (such as a gel) are neglected by the PBE but are very important.^{10,21} Consequently, higher-order terms are neglected from eqs 1 and 2, permitting the formation of ∞ -mers (from mass continuity) and the definition of a specific time at which the gel forms. Because the stochastic approach is mathematically equivalent to the stochastically exact PBE,¹¹ it should be expected that the higher-order terms in such stochastically exact PBEs preclude the divergence of the second- and higher-order moments of the size distribution.

Thus, whereas the gel transition in single-component systems is customarily defined as the time at which the second moment $M_2(t)$ diverges with a concomitant decrease in total mass $M_1(t)$, Figures 3–5 show a clear gel transition without such a divergence. Moreover, the

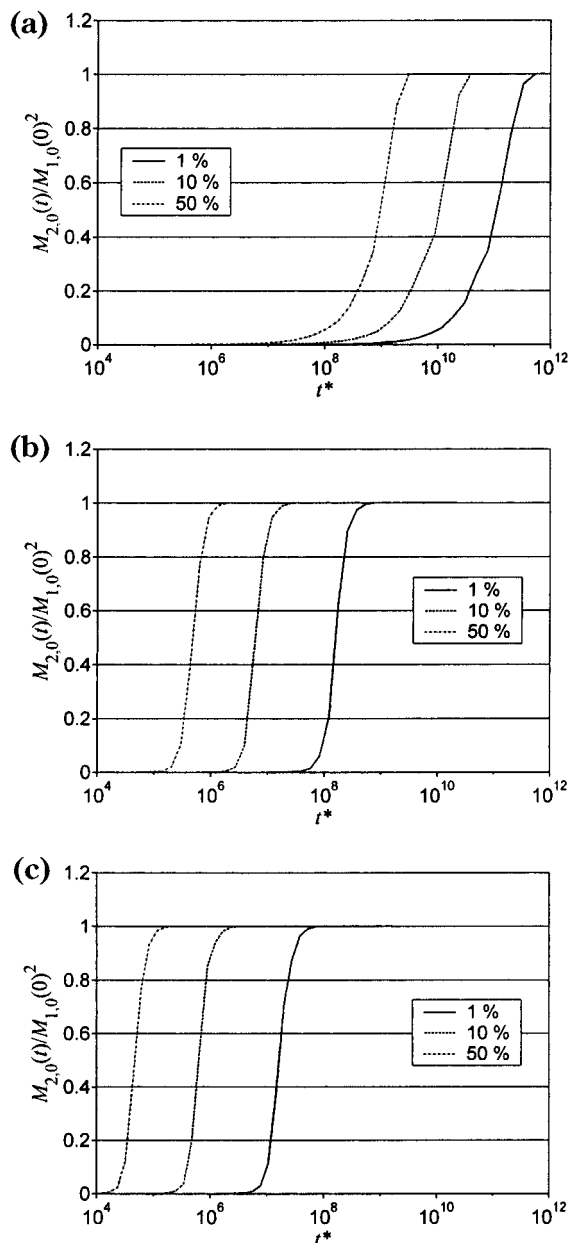


Figure 3. Normalized second moment of particle distribution in the small component ($M_{2,0}$) at shear rates $G =$ (a) 0, (b) 1.0, and (c) 10.0 s^{-1} . The beginnings of the rapid increases reflect the formation of a gel.

MC algorithm forces conservation of mass, such that $M_{1,0}(t) \equiv M_{1,0}(0)$ and $M_{0,1}(t) \equiv M_{0,1}(0)$. Figures 3–5 show that the gel transition in the real system occurs just before the rapid growth of the second moments late in the aggregation process, when about 90% of the particles have aggregated. Supporting this result is the fact that the rapid growth phase begins at the same time in Figures 3–5 at each shear rate and ξ . Thus, the results indicate that the real gel point of an aggregating system of arbitrary components is characterized by a rapid and finite increase in the second moments, asymptotically approaching unity. This result has been previously demonstrated, albeit in a different form, in MC simulations of polymerization kernels with known gel points.²² Moreover, Figures 3a, 4a, and 5a show that, in the absence of shear, no gel formation (rapid increase of the second moments) distinct from complete aggregation is observed. In this case, the growth of the second moment

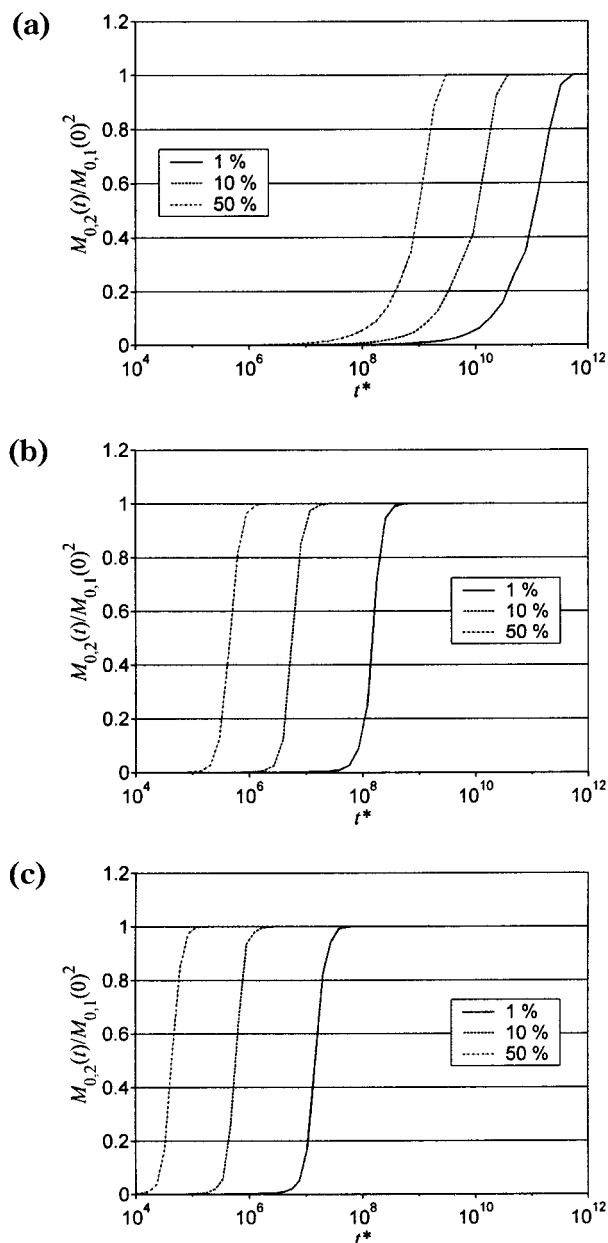


Figure 4. Normalized second moment of particle distribution in the large component ($M_{0,2}$) at shear rates $G =$ (a) 0, (b) 1.0, and (c) 10.0 s^{-1} .

to unity requires decades, whereas the shear-mediated process is rapid.

Figures 3–5 also show the effects of seeding the small particles of the first component with larger particles of the second. Although the speed of the gel transition is greatly enhanced by the addition of large particles, there are diminishing returns with respect to this addition. For example, gel points occur about 20–30 times faster as ξ is increased from 1 to 10%. An increase in ξ from 10 to 50% diminishes the gel point by an additional factor of about 13, regardless of the shear rate. In summary, these results indicate that the addition of microscopic particles to Brownian particles increases the total rate of aggregation by increasing the shear sensitivity of the process. Consequently, by addition of a small amount of microscopic particles, an aggregation of Brownian particles can be enhanced or controlled by shear. The method provided in this work gives exact quantification of these concentration and shear dependencies.

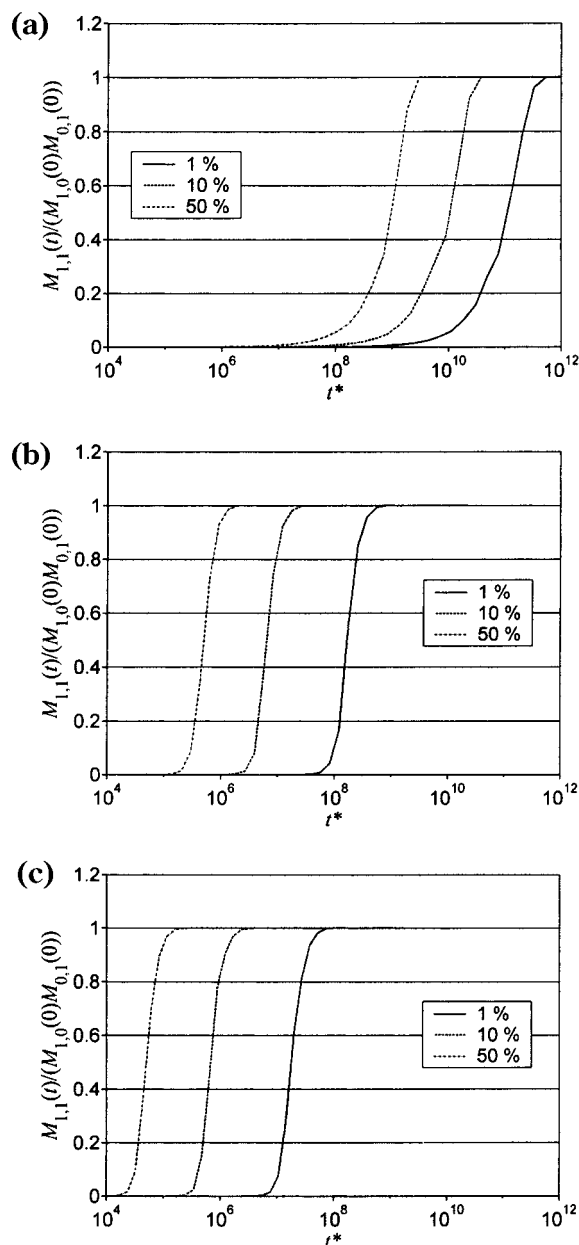


Figure 5. Normalized mixed second moment $M_{1,1}$ of particle distribution at shear rates $G =$ (a) 0, (b) 1.0, and (c) 10.0 s^{-1} .

Conclusions

By use of a stochastic approach to aggregation kinetics, an exact multicomponent analysis of irreversible transport-limited aggregation via combined Brownian motion and shear has been performed for the first time. Because the stochastic approach is based on the microphysics of the aggregation process and lacks the mathematical complexity of Smoluchowski's and Lushnikov's equations, it permits MC simulation of any aggregation kernel with any initial distribution of particles, regardless of the number of components or complexity of the kernel. Furthermore, it gives a more exact mathematical treatment of gel formation and its characterization.

Aggregation simulations of two types of volumetrically polydisperse single-component particles with a diameter ratio of 1:8 were performed at the size scale spanning the Brownian and shear-mediated transport mechanisms. The results demonstrated the capacity of shear and seeding with large particles to augment the speed

of aggregation and hasten gelation. In the absence of shear, no gel transition was observed. However, even at small shear rates, gel formation was observed, where the gel point was shown to be rapid, but not instantaneous, and strongly dependent on shear rate. Furthermore, neither divergence of the second-order moments nor decrease of the first moments of the particle size distribution were observed at or after the gel point.

Seeding with micron-sized particles was shown to increase the sensitivity of the aggregation process to mixing and hasten the process of gelation of the Brownian aggregation process by orders of magnitude. However, in the absence of shear, the consumption of particles was essentially independent of the large particles. Furthermore, the benefits of seeding diminish as the initial fraction of particles of micron-size increases beyond 10%, especially at large shear rates. Whereas the cooperative effects of seeding and shear can be used to control the gel point, other design parameters such as shear- and composition-dependent sticking probabilities can also be analyzed by MC simulation.

Acknowledgment

This work was supported by National Institutes of Health Grant HL 56621 and National American Heart Association Grant 96-6670. S.L.D. is an Established Investigator of the National American Heart Association.

Notation

- \mathcal{A} = transition matrix of an aggregating system
- $a(i, j)$ = frequency of aggregation between any particles of species i and j
- $C(i, j)$ = frequency of aggregation between specific particles of species i and j
- $c(i, t)$ = concentration of i -mers at time t
- $\check{c}(u, v, t)$ = bivariate concentration distribution density
- c_0 = total initial concentration of particles
- c_1, c_2 = initial concentrations of pure particles of components 1 and 2, respectively
- $G(u, v, t)$ = cumulative concentration distribution
- $K(i, j)$ = aggregation kernel between i -mers and j -mers or between species i and j
- $K(u, v | u_1, v_1)$ = bivariate aggregation kernel
- k_B = Boltzmann's constant
- \mathcal{M}, \mathcal{N} = number of abscissas for initial discretization of component 1 and 2 size/mass spaces
- $M_{ij}(t)$ = (i, j) -th moment of bivariate population distribution
- N = number of particle species
- \mathcal{P} = vector of the probabilities of states of an aggregating system
- $Pe_{i,j}$ = Peclet number between components i and j
- r_2, r_1 = random numbers
- R_1, R_2 = radii of pure particles of components 1 and 2, respectively
- T = temperature
- t = time
- u, u_1 = size/mass of component 1 in aggregating particles
- u_j, v_k = abscissas of the size/mass spaces of components 1 and 2
- \bar{u}_k, \bar{v}_k = size/mass of components 1 and 2 in species k
- v, v_1 = size/mass of component 2 in aggregating particles
- V = batch volume
- X_0 = initial number of particles
- X_i = population of species i
- α = total aggregation frequency

α_1, α_2 = size factors for gamma distributions of size for components 1 and 2, respectively
 β_1, β_2 = shape factors for gamma distributions of size for components 1 and 2, respectively
 $\epsilon(u, v|u_1, v_1)$ = sticking probability
 η = solution viscosity
 ϕ = volume fraction of aggregating particles
 μ, ν = indices of species that will imminently aggregate
 τ = quiescence time
 ξ = number fraction of initial particles composed of component 2

Appendix: Monte Carlo Sampling of a Bivariate Probability Distribution

The MC selection of abscissas X and Y from a bivariate probability distribution density can be performed as follows: Consider a distribution density $P(x, y)$ with $x \in [a, b]$ and $y \in [a', b']$, where any of a, a', b or b' can be infinite. If $P(x, y)$ is a normalized density function, it obeys the equation

$$\text{Prob}(X, Y; X \leq x, Y \leq y) = \int_{a'}^y \int_a^x P(x, y) \, dx \, dy \leq 1 \quad (22)$$

The Monte Carlo method of sampling the distribution is to define a probability via a random number generator and set it equal to the cumulative distribution. In the case of a bivariate distribution, proper conditioning must be employed to obtain independent results. Thus, one can define

$$\text{Prob}(X; X < x \leq b) = \int_{a'}^b \int_a^x P(x, y) \, dx \, dy \quad (23)$$

as the probability that $X \leq x$ and

$$\text{Prob}(Y|X; Y \leq y|X \leq x) = \int_{a'}^y \int_a^x P(x, y) \, dx \, dy / \int_{a'}^b \int_a^x P(x, y) \, dx \, dy \quad (24)$$

as the probability that $Y \leq y$, given that $X \leq x$. The product of these probabilities gives eq 22. Consequently, a value of X can be selected by setting the LHS of eq 23 to a uniformly generated random number $r \in [0, 1]$. With $X = x$ chosen, subsequent selection of a value of Y can be performed likewise, but with a different random number.

Literature Cited

(1) Friedlander, S. K. *Smoke, Dust and Haze—Fundamentals of Aerosol Dynamics*, 2nd ed.; Oxford University Press: New York, 2000.

(2) Laurenzi, I. J.; Diamond, S. L. Monte Carlo Simulation of the Heterotypic Aggregation Kinetics of Platelets and Neutrophils. *Biophys. J.* **1999**, *77*, 1733.

(3) Konstantopoulos, K.; Neelamegham, S.; Burns, A. R.; Hentzen, E.; Kansas, G. S.; Snapp, K. R.; Berg, E. L.; Hellums, J. D.; Smith, C. W.; McIntire, L. V.; Simon, S. I. Venous Levels of Shear Support Neutrophil-Platelet Adhesion and Neutrophil Aggregation in Blood via P-Selectin and Beta(2)-Integrin. *Circulation* **1998**, *98*, 873.

(4) Smoluchowski, M. v. Versuch Einer Mathematischen Theorie der Koagulation Kinetic Kolloider Lösungen. *Z. Phys. Chem.* **1917**, *92*, 129.

(5) Lushnikov, A. A. Evaluation of Coagulating Systems III: Coagulating Mixtures. *J. Colloid Interface Sci.* **1976**, *54*, 94.

(6) McLeod, J. B. On an Infinite Set of Nonlinear Differential Equations. *Q. J. Math. (Oxford)* **1962**, *2*, 119.

(7) Golovin, A. M. The Solution of the Coagulation Equation for Cloud Droplets in a Rising Air Current. *Bull. (Izv.) Geophys. Sci.* **1963**, 482.

(8) Scott, W. T. *Analytical Studies of Cloud Droplet Coalescence I*; DRI Technical Report 9; University of Nevada: Reno, NV, 1965.

(9) Laurenzi, I. J.; Bartels, J. D.; Diamond, S. L. A General Algorithm for Exact Simulation of Multi-Component Aggregation, manuscript submitted.

(10) McQuarrie, D. A. Stochastic Approach to Chemical Kinetics. *J. Appl. Prob.* **1967**, *4*, 413.

(11) Gillespie, D. T. The Stochastic Coalescence Model for Cloud Droplet Growth. *J. Atmos. Sci.* **1972**, *29*, 1496.

(12) Gillespie, D. T. A General Method for Numerically Simulating the Stochastic Time Evolution of Coupled Chemical Reactions. *J. Comput. Phys.* **1976**, *22*, 403.

(13) Gillespie, D. T. Exact Stochastic Simulation of Coupled Chemical Reactions. *J. Chem. Phys.* **1977**, *81*, 2340.

(14) Feke, D. L.; Schowalter, W. R. The Effect of Brownian Diffusion on Shear-Induced Coagulation of Colloidal Dispersions. *J. Fluid Mech.* **1983**, *133*, 17.

(15) Tandon, P.; Diamond, S. L. Hydrodynamic Effects and Receptor Interactions of Platelets and Their Aggregates in Linear Shear Flow. *Biophys. J.* **1997**, *73*, 2819.

(16) van de Ven, T. G. M.; Mason, S. G. The Microrheology of Colloidal Dispersions VIII. Effect of Shear on Perikinetic Doublet Formation. *Colloid Polym. Sci.* **1977**, *255*, 794.

(17) Swift, D. L.; Friedlander, S. K. The Coagulation of Hydrogels by Brownian Motion and Laminar Shear Flow. *J. Colloid Sci.* **1964**, *19*, 621.

(18) Oles, V. Shear-Induced Aggregation and Breakup of Polystyrene Latex Particles. *J. Colloid Interface Sci.* **1992**, *154*, 351.

(19) Spicer, P. T.; Pratsinis, S. E. Coagulation and Fragmentation: Universal Steady-State Particle-Size Distribution. *AIChE J.* **1996**, *42*, 1612.

(20) Serra, T.; Colomer, J.; Casamitjana, X. Aggregation and Breakup of Particles in a Shear Flow. *J. Colloid Interface Sci.* **1997**, *187*, 466.

(21) Laurenzi, I. J. An Analytical Solution of the Stochastic Master Equation for Reversible Bimolecular Reaction Kinetics. *J. Chem. Phys.* **2000**, *113*, 3315.

(22) Spouge, J. L. Monte Carlo Results for Random Coagulation. *J. Colloid Interface Sci.* **1985**, *107*, 38.

Received for review February 28, 2001

Revised manuscript received October 1, 2001

Accepted October 2, 2001

IE010197J